

Anomalous and nonlinear Hall effects in two-dimensional CrPS₄

Lulu Xiong,¹ Jin Cao,^{1,*} Fan Yang,² Xiaoxin Yang,¹ Shen Lai,^{1,†}
Xian-Lei Sheng,^{2,3} Cong Xiao,^{1,‡} and Shengyuan A. Yang¹

¹*Institute of Applied Physics and Materials Engineering,
University of Macau, Taipa, Macau SAR, China*

²*School of Physics, Beihang University, Beijing 100191, China*

³*Peng Huanwu Collaborative Center for Research and Education, Beihang University, Beijing 100191, China*

Few-layer CrPS₄ is a two-dimensional (2D) magnetic material with excellent stability in ambient environment, which attracted significant interest in recent research. Here, via first-principles calculations, we show that 2D CrPS₄ hosts a variety of anomalous Hall transport phenomena, owing to its layer-dependent magnetism and symmetry character. Monolayer CrPS₄ can display a sizable linear anomalous Hall effect, while its nonlinear anomalous Hall response is forbidden. In contrast, bilayer CrPS₄ can produce pronounced intrinsic nonlinear anomalous Hall response from Berry-connection polarizability, in the absence of linear anomalous Hall effect. We clarify that the large peaks in these responses originate from gapped Dirac points in the band structure. Furthermore, we show that linear anomalous Hall effect can be induced and controlled in bilayer CrPS₄ by gate electric field or in-plane magnetic field, which break the spacetime inversion symmetry. Our findings unveil the interesting layer-dependent Hall transport physics in 2D CrPS₄ magnets, suggesting its potential in electronic and spintronic device applications.

I. INTRODUCTION

The various Hall effects are of fundamental importance in condensed matter physics. A prominent example is the (linear) anomalous Hall effect (AHE), where a Hall voltage is induced by a longitudinal current flow in a magnetic material [1]. An important advance in the past two decades is the recognition that this effect contains an intrinsic contribution, i.e., an response determined solely by the material's band structure, which manifests an intriguing band geometric property, the Berry curvature of electronic bands [2, 3]. AHE is a time-reversal-odd (\mathcal{T} -odd) effect, meaning that reversal of magnetic moments in the system (corresponding to a time-reversal operation) must flip the sign of the response coefficient. The \mathcal{T} -odd Hall effect was also discovered in nonlinear response of magnets, giving a Hall current quadratic in the driving E field, i.e., $j_H \propto E^2$ [4–6]. Importantly, this nonlinear AHE also contains an intrinsic contribution, which is determined by another band geometric quantity, the Berry-connection polarizability (BCP) [6, 7], and can be further connected to the quantum metric of band structure [5, 8, 9]. Note that this effect is distinct from the \mathcal{T} -even nonlinear AHE that has been widely studied in nonmagnetic materials and does not have an intrinsic contribution [10–13]. Recently, such intrinsic nonlinear AHE has been experimentally detected in a few magnets, such as few-layer MnBi₂Te₄ [8, 14] and Mn₃Sn [15].

Meanwhile, a focus of current materials research is to explore two-dimensional (2D) magnets [16–18]. Several material classes, like CrI₃ [19], Fe₃GeTe₂ [20, 21],

Cr₂Ge₂Te₆ [22], and MnBi₂Te₄ [23, 24], have been realized. Due to the reduced dimensionality, a big advantage of 2D magnets is that their properties can be flexibly tuned, e.g., by gating, doping, strain, external fields, and hetero-structure engineering. Nevertheless, it was noted that most of 2D magnets studied so far are not stable in ambient environment, posing difficulties for applications. In this regard, the recently realized 2D magnet CrPS₄ starts to attract increasing attention because of its excellent air stability [25]. It was shown that its magnetic ordering can persist down to monolayer limit [25]. The physical properties of CrPS₄, such as spin dynamics, layer-dependent magnetism, optical response, electric and thermal transport properties, have been studied in several recent works [25–37]. As a semiconductor, the type and density of its charge carriers can be conveniently controlled by gating [35, 36]. Devices based on 2D CrPS₄, such as field effect transistors and magnetic tunnel junctions, have been studied in experiment [36–38].

Here, we note that 2D CrPS₄ actually offers a good platform to study a variety of Hall effects. First, 2D CrPS₄ with odd number of layers is ferromagnetic (FM), which allows linear AHE. Second, even-layer CrPS₄ has a compensated antiferromagnetic (AFM) ordering, which preserves spacetime inversion (\mathcal{PT}) symmetry. This forbids the linear AHE. However, the intrinsic nonlinear AHE is permitted. It should be noted that the symmetry condition of this nonlinear effect in 2D systems is a bit stringent: It requires the absence of any out-of-plane rotation axis [5, 6]. CrPS₄ naturally satisfies this condition due to its monoclinic crystal structure. Third, although linear AHE is forbidden in the ground state of even-layer CrPS₄, external fields may break the \mathcal{PT} symmetry and generate a field-induced AHE.

Motivated by these considerations, in this work, we perform a study of the various Hall responses in 2D CrPS₄ via first-principles calculations. We focus on

* caojin.phy@gmail.com

† laishen@um.edu.mo

‡ xiaoziche@gmail.com

monolayer and bilayer CrPS₄ as representatives. For monolayer CrPS₄, we show that it has a sizable anomalous Hall conductivity in the case of hole doping. Its value can be strongly influenced by the magnetization direction. For bilayer CrPS₄, we show that the intrinsic nonlinear AHE is determined by a single response coefficient, which can achieve a large value ~ 1 mA/V² under hole doping. The origin of the large contribution in BCP is traced to a band anti-crossing region in valence bands. Furthermore, to induce linear AHE in bilayer CrPS₄, we break the \mathcal{PT} symmetry in two ways. The first is by a gate electric field (in the out-of-plane direction). The resulted net AHE response has a sign determined by the gate field direction, and the Hall current has a dominant distribution in one of the layers. The second way is to apply an in-plane magnetic field, which causes canting of the local moments and leads to an in-plane magnetization. We show that the resulting AHE can be quite large under moderate applied field strength. The two methods are also discussed from the perspective of layer Hall effect. Our results reveal interesting Hall transport physics in the 2D magnet CrPS₄, which may find potential applications in novel electronic and spintronic devices.

II. COMPUTATION METHOD

Our first-principles calculations based on density functional theory (DFT) were performed by using Vienna *ab-initio* simulation package [39–41], employing the projector augmented wave pseudo-potentials [42]. The exchange-correlation energy was treated with the generalized-gradient approximation [43] in the scheme of the Perdew-Burke-Ernzerhof realization [44]. To account for van der Waals (vdW) interactions, the DFT-D3 method was adopted [45]. The Dudarev *et al.*'s approach [46] was used to treat possible correlation effects of Cr-3*d* orbitals. Following Ref. [25], we took effective U value to be 2 eV, which gives magnetic moment and bandgap values consistent with experiment. The plane-wave cutoff energy was set to 400 eV, and a k -point mesh with size $12 \times 12 \times 1$ was used for the Brillouin zone (BZ) sampling. For 2D layers, a vacuum space of thickness 18 Å was added to suppress artificial interactions among periodic images. The convergence criteria for the total energy and the force were set to 10^{-6} eV and 0.01 eV/Å, respectively. The spin-orbit coupling was included in all calculations. Based on DFT results, *ab-initio* tight-binding models were constructed by using the Wannier90 package [47], which were then used for computing band geometric quantities and transport coefficients.

III. STRUCTURE AND MAGNETIC ORDERING

Bulk CrPS₄ is a vdW layered material with monoclinic crystal structure belonging to the $C2/m$ space group

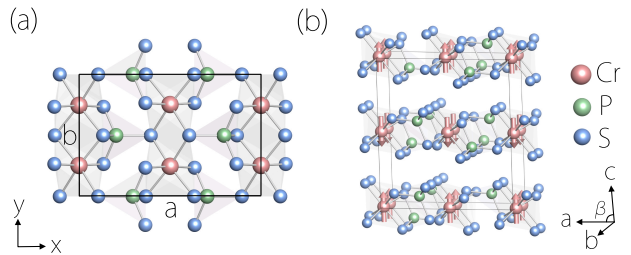


FIG. 1. (a) Top view of a CrPS₄ layer. The black rectangle marks the conventional cell. (b) Lattice structure of bulk CrPS₄. It has a A -type AFM ground state. The local moments are in the out-of-plane direction, as indicated by the red arrows in the figure.

(see Fig. 1). It was first synthesized and studied in the 1970s [48]. A recent experimental characterization reported that its lattice parameters (for the conventional cell) are $a = 10.856$ Å, $b = 7.247$ Å, and $c = 6.135$ Å [29]. As shown in Fig. 1(a), in a layer, each Cr cation is surrounded by six S anions, forming a CrS₆ octahedron with slight Jahn-Teller distortion. These CrS₆ octahedra form quasi-1D chains along y direction in Fig. 1(a), which are further inter-connected by PS₄ tetrahedra, resulting in a rectangle lattice in the 2D plane. Due to the relatively weak vdW interaction, a slight slip along a axis direction occurs between neighboring layers, causing angle $\beta = 88.116^\circ$, which deviates slightly from 90° (see Fig. 1(b)). The bulk structure of CrPS₄ preserves the spatial inversion symmetry \mathcal{P} . However, due to the in-plane anisotropy as described above, there is no vertical rotation axis (only a twofold axis along y exists).

The magnetic ground state of CrPS₄ is well established in previous studies [25, 29]. The magnetism comes mainly from the Cr³⁺ ions with a magnetic moment about $3.0\mu_B$. The magnetic coupling within each layer is FM and the moments are in the out-of-plane direction; whereas the coupling between neighboring layers is AFM. This results in an overall A -type AFM ordering for bulk CrPS₄, with Néel vector along z axis, as shown in Fig. 1(b). The Néel temperature reported in experiment is about 35 to 38 K [25, 28–30, 38].

As a vdW layered material, 2D few layers can be easily exfoliated from bulk CrPS₄. Experimentally, 2D CrPS₄ with thickness down to monolayer has been successfully fabricated, via mechanical exfoliation or thermal atomic layer etching method [25]. Compared to other 2D magnets, a big advantage of this material is its good stability in air. It was shown that the magnetism is robust down to monolayer limit, and the ground state exhibits a layer-dependent alternation between two configurations. The odd layers are uncompensated antiferromagnet with a net magnetization along z (FM for monolayer), whereas the even layers feature a fully compensated AFM state. The magnetic transition temperature shows a slight decrease when thickness decreases. The transition temperature for monolayer is found to be ~ 22 K [25]. Taking into ac-

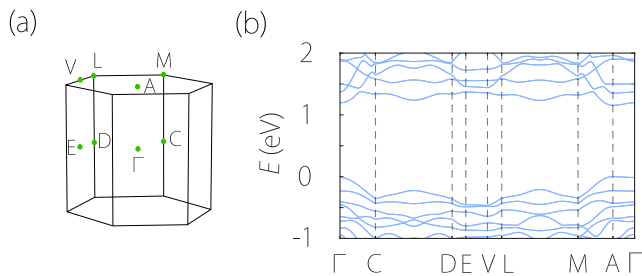


FIG. 2. (a) Brillouin zone and (b) calculated band structure for bulk CrPS₄.

count the ground state magnetic configuration, the odd layers have $2'/m'$ magnetic point group, whereas the even layers belong to $2/m'$. Their key difference is that the odd layers preserve \mathcal{P} (not \mathcal{PT}), but the even layers preserve \mathcal{PT} (not \mathcal{P}). This has important consequences on the type of Hall effects allowed in the system, as we shall discuss in a while.

The band structure for bulk CrPS₄ in the AFM ground state obtained from our DFT calculation is plotted in Fig. 2(b). The result shows that CrPS₄ is a magnetic semiconductor. The obtained bandgap value ~ 1.21 eV agrees very well with the recent experimental result (~ 1.31 eV) [28]. Our calculated magnetic moment $\sim 3.0\mu_B$ on Cr site also agrees with several previous experiments [25, 29]. These support the validity of our computation method. In the case of few layers, we find that they are also magnetic semiconductors. The local magnetic moments remain nearly unchanged compared to the bulk. These features are consistent with previous studies. In the following, we shall focus on monolayer and bilayer CrPS₄ to study their various Hall responses.

IV. ANOMALOUS HALL RESPONSE IN MONOLAYER

Due to *A*-type magnetic ordering, odd-layer CrPS₄ has an uncompensated net magnetization. For monolayer CrPS₄, this reduces to the FM ordering, with all magnetic moments in the out-of-plane direction (*z* direction in our setup). The band structure for this ground state is plotted in Fig. 3(c). The result shows a semiconductor with a bandgap ~ 1.20 eV, which agrees with previous studies [25].

As we noted above, the magnetic point group for monolayer CrPS₄ (with FM ordering) is $2'/m'$, which consists of two elements: \mathcal{P} and \mathcal{TM}_y (\mathcal{M}_y is the mirror normal to *y*). This symmetry allows for a nonzero σ_{xy} for linear AHE. On the other hand, any nonlinear charge transport, including nonlinear Hall effect, is forbidden.

Here, we compute the intrinsic AHE response. The corresponding anomalous Hall conductivity is given

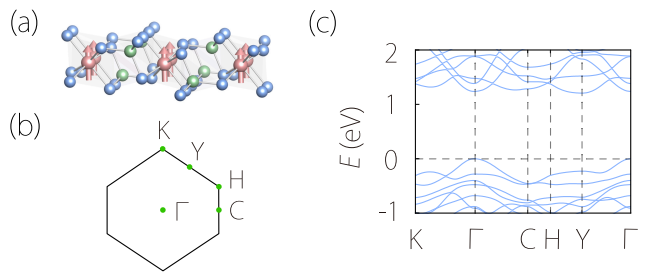


FIG. 3. (a) Lattice structure of monolayer CrPS₄, which has FM ordering with out-of-plane magnetization. (b) Brillouin zone of the monolayer. (c) Band structure for monolayer CrPS₄ in the FM ground state.

by [49, 50]

$$\sigma_{xy} = \frac{e^2}{\hbar} \int [d\mathbf{k}] f_{n\mathbf{k}} \Omega_z^n(\mathbf{k}), \quad (1)$$

where $[d\mathbf{k}]$ is the short notation of $\sum_n d\mathbf{k}/(2\pi)^2$, n is the band index, $f_{n\mathbf{k}}$ is the Fermi-Dirac distribution function, and

$$\Omega_z^n(\mathbf{k}) = -2\hbar^2 \text{Im} \sum_{m \neq n} \frac{(v_x)_{nm}(v_y)_{mn}}{(\varepsilon_n - \varepsilon_m)^2} \quad (2)$$

is the Berry curvature of Bloch band structure, with ε_n being the band energy and $(v_i)_{mn}$ being the interband velocity matrix element. For simple notations, we suppress the k dependence in Eq. (2) above. From Eq. (1), one can see that this AHE response is intimately connected to Berry curvature of occupied states.

In Fig. 4(a), we show the calculation result of σ_{xy} as a function of the chemical potential μ . One can observe several peaks in both hole-doped and electron-doped regions. The peak at $\mu \sim -0.32$ eV can reach up to ~ -600 S/cm, which is a quite large value. To understand the origin of this peak, we calculate the Berry curvature distribution in k space summed over states below -0.32 eV. The result is shown in Fig. 4(b). One can see that large Berry curvature comes from two hot spots sitting on the Γ - K path. These hot spots correspond to the small-gap regions indicated in Fig. 4(c). It should be noted that here, the two bands do not cross, instead, they form an anti-crossing with a small gap ~ 0.014 eV. Such anti-crossing may be considered as a 2D gapped Dirac point. From symmetry analysis, we construct the following $k \cdot p$ effective model for this gapped Dirac point:

$$H_{\text{eff}} = wk_y + v_x k_x \tau_y + v_y k_y \tau_z + m \tau_x, \quad (3)$$

where momentum k is measured from the Dirac point, τ 's are Pauli matrices, w , v_i , and m are real model parameters. It is known that Berry curvature is concentrated around such points, where the interband coherence is strong. This explains the feature that we observe in Fig. 4(c).

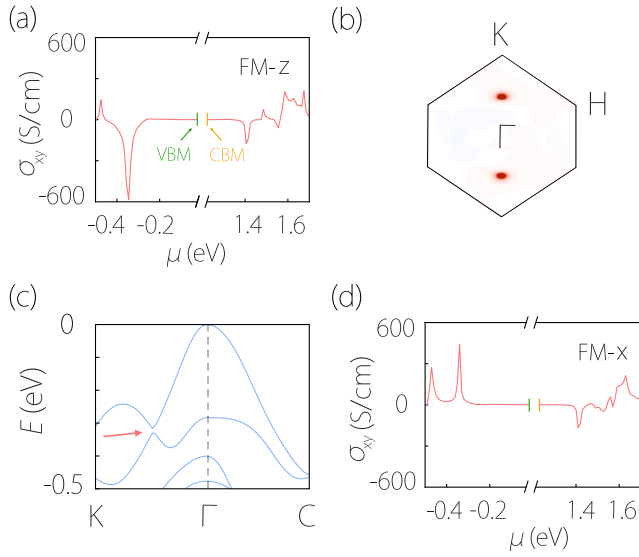


FIG. 4. (a) Calculated intrinsic anomalous Hall conductivity for monolayer CrPS₄ as a function of chemical potential. (b) Distribution of Berry curvature for states below $\mu = -0.32$ eV. (c) The hot spots in (b) correspond to the gapped Dirac points in band structure. The red arrow indicates one point. The other one is related to this one by inversion symmetry. (d) The result of intrinsic anomalous Hall conductivity when the magnetization is rotated to be along the x direction.

The magnetic anisotropy in 2D CrPS₄ is not very large. It was shown in experiment that the magnetic moment direction can be rotated by relatively small applied magnetic field ~ 90 mT [25]. Hence, we also consider the AHE response in monolayer when the magnetization is rotated to an in-plane direction. In Fig. 4(d), we show the calculated σ_{xy} for magnetization along the x direction. Again, several peaks can be observed in the figure. The peak values are comparable to those in Fig. 4(a). The first peak in valence band has a value ~ 370 S/cm. Furthermore, for magnetization along y direction, σ_{xy} is identically zero. This is because in this configuration, the vertical mirror \mathcal{M}_y symmetry is preserved, which forbids the AHE.

V. NONLINEAR HALL RESPONSE IN BILAYER

For the even-layer CrPS₄, the state above Néel temperature T_N possesses both \mathcal{P} and \mathcal{T} symmetries, which prohibit linear AHE and any second order current response. Below T_N , the AFM state preserves \mathcal{PT} symmetry, so that the linear AHE is still suppressed, however, the nonlinear Hall response starts to appear. This nonlinear response can be expressed as

$$\hat{j}_a = \chi_{abc} E_b E_c, \quad (4)$$

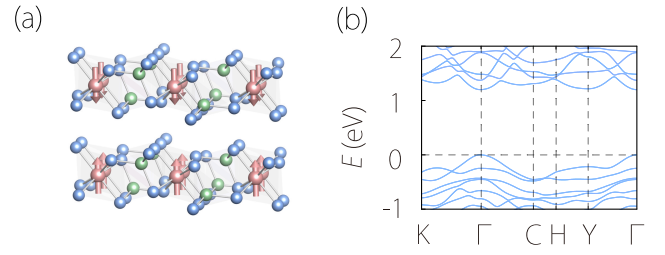


FIG. 5. (a) Lattice structure of bilayer CrPS₄, which has A-type AFM ground state. (b) Calculated band structure for bilayer CrPS₄ in AFM ground state.

where χ_{abc} is the nonlinear conductivity tensor, the subscripts label the Cartesian components, and the Einstein summation convention is assumed here. Here, we focus on the intrinsic contribution to nonlinear Hall transport, which is determined solely by the band structure property. It should be noted that the extrinsic contribution from Berry curvature dipole is forbidden by the \mathcal{PT} symmetry here [10].

The theory of intrinsic nonlinear Hall effect has been developed in Ref [4–6]. The corresponding nonlinear conductivity tensor can be expressed as

$$\chi_{abc} = \frac{e^2}{\hbar} \int [d\mathbf{k}] f_{n\mathbf{k}} \Lambda_{abc}^n(\mathbf{k}) \quad (5)$$

where

$$\Lambda_{abc}^n(\mathbf{k}) = \partial_b G_{ac}^n - \partial_a G_{bc}^n \quad (6)$$

is the k -resolved BCP dipole, and

$$G_{ab}^n(\mathbf{k}) = 2e\hbar^2 \text{Re} \sum_{m \neq n} \frac{(v_a)_{nm} (v_b)_{mn}}{(\varepsilon_n - \varepsilon_m)^3} \quad (7)$$

is the BCP tensor, and $\partial_a \equiv \partial_{k_a}$. Like Berry curvature, BCP is a gauge-invariant quantity. Physically, it characterizes the shift of a electron wavepacket center by an applied electric field [4]. Near hot spots formed by a pair of bands, BCP can be further connected to the quantum metric of band structure [9].

In the following, we focus on the bilayer CrPS₄ as a representative. The calculated band structure is plotted in Fig. 5(b). It should be noted here that each band is doubly spin degenerate due to the \mathcal{PT} symmetry. As for the nonlinear conductivity tensor, we note that the $2/m'$ symmetry of the system dictates that the intrinsic response is characterized by a single independent component, with

$$\chi_{yxx} = -\chi_{xyx}. \quad (8)$$

For an in-plane E field in the direction $\mathbf{E} = E(\hat{x} \cos \phi + \hat{y} \sin \phi)$, where ϕ is the polar angle measured from x axis, the resulting Hall current j_H in the direction normal to E field can be expressed as

$$j_H = \chi_H(\phi) E^2, \quad \chi_H(\phi) = \chi_{yxx} \cos \phi. \quad (9)$$

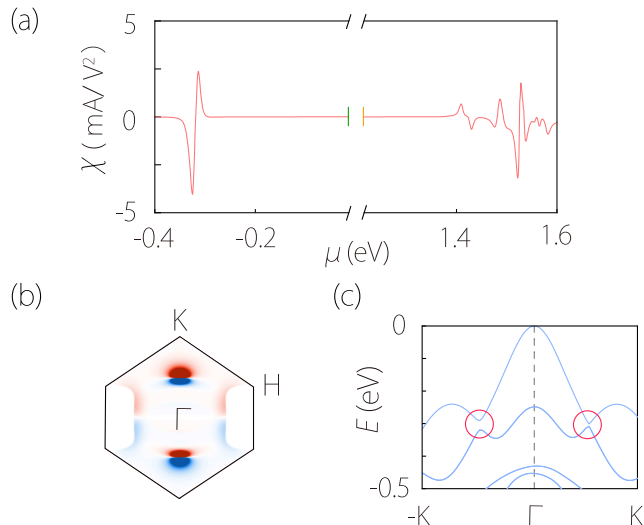


FIG. 6. (a) Calculated intrinsic nonlinear Hall conductivity χ_{yxx} as a function of chemical potential for bilayer AFM CrPS₄. (b) k -space distribution of BCP dipole for states below $\mu = -0.3$ eV. The hot spots on Γ - K path correspond to the two gapped Dirac points marked in the enlarged band structure in (c).

In nonlinear Hall experiment, one typically fabricate a disk shaped device and multiple leads, such that the driving current can be applied along various in-plane directions while measuring the Hall response in the transverse direction [12, 51]. Equation (9) tells us the angular dependence of the measured Hall signal should exhibit a simple cosine dependence, with a 2π periodicity.

Next, we compute the nonlinear conductivity component χ_{yxx} from our DFT result. The result is shown in Fig. 6(a). One observes that the value on the electron-doping side can reach ~ 0.4 mA/V². For hole doping, the peak at $\mu = -0.3$ eV is even larger, reaching ~ 2 mA/V², which is quite large. It is comparable to the one measured in few-layer MnBi₂Te₄ [8, 52].

To reveal the origin of this peak, we plot the distribution of k -resolved BCP dipole $\Lambda_{yxx}(\mathbf{k})$ in BZ by summing over all occupied states up to $\mu = -0.3$ eV. The result is plotted in Fig. 6(b). One can see a pronounced dipole like distribution in a small region around a point on Γ - K ($k_y > 0$) path. This corresponds to a band anti-crossing point as indicated in Fig. 6(c). By analyzing the band structure around this point, we identify it as a gapped Dirac point. However, different from that in Fig. 4(d), the bands are doubly degenerate. The effective model for this point from symmetry analysis takes the following form:

$$H_{\text{eff}} = wk_y + v_x k_x (\sigma_x \cos \alpha + \sigma_y \sin \alpha) \tau_y + v_y k_y \sigma_z \tau_y + m \tau_x, \quad (10)$$

where the wavevector k is measured from the point, σ and τ are two sets of Pauli matrices, w , v 's, α , and m are real model parameters. The last term in (10) opens a

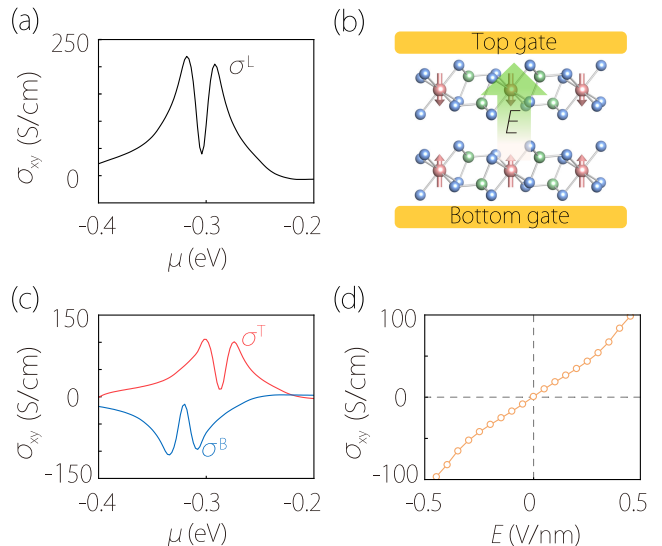


FIG. 7. (a) Calculated layer Hall conductivity in bilayer CrPS₄. Here, we focus on the peak structure in valence band. (b) Schematic figure showing the application of a gate electric field to bilayer CrPS₄. This breaks the \mathcal{PT} symmetry and generates a finite anomalous Hall response. (c) Layer-resolved Hall conductivities under a gate field of 0.02 V/nm. (d) The resulting anomalous Hall conductivity versus gate field at a fixed chemical potential of -0.25 eV.

small gap ~ 0.007 eV between the two doubly degenerate bands. As shown in Ref. [5, 6], such gapped Dirac point tends to enhance BCP hence makes significant contribution to the nonlinear Hall response. In Fig. 6(c), there is another hot spot on the $k_y < 0$ portion of Γ - K path, with a comparatively weaker BCP dipole distribution. This corresponds to another gapped Dirac point at energy slightly below -0.3 eV (see Fig. 6(b)). The form of its effective model is the same as Eq. (10), since the local symmetry is the same.

VI. LAYER HALL EFFECT IN BILAYER

We have shown that a large AHE can be realized in monolayer CrPS₄. The bilayer is made of two monolayers with opposite magnetization. Hence, the vanishing of AHE in bilayer can be intuitively understood as the exact cancellation of the AHE responses of the two monolayers. From this perspective, one may consider the bilayer system actually hosts a layer Hall effect [53], i.e., the AHE response is finite in each layer channel and is opposite between the two channels. This is analogous to concepts of the spin Hall effect and valley Hall effect, with layer index being the binary degree of freedom.

Similar to spin or valley Berry curvature, we may define a layer Berry curvature [54] for bilayer CrPS₄:

$$\Omega_z^{n,\ell}(\mathbf{k}) = -2\hbar^2 \text{Im} \sum_{m \neq n} \frac{(v_x^\ell)_{nm} (v_y^\ell)_{mn}}{(\epsilon_n - \epsilon_m)^2}, \quad (11)$$

where $\ell = T, B$ is the binary layer index for top and bottom layers, $(v_x^\ell)_{nm}$ is the interband matrix element for the operator $\hat{v}_x^\ell = \{\hat{P}_\ell, \hat{v}_x\}/2$, i.e., the velocity operator combined with the projector \hat{P}_ℓ into layer ℓ . The response of AHE in each layer is characterized by

$$\sigma_{xy}^\ell = \frac{e^2}{\hbar} \int [d\mathbf{k}] f_{n\mathbf{k}} \Omega_z^{n,\ell}(\mathbf{k}). \quad (12)$$

One can easily see that the total anomalous Hall conductivity

$$\sigma_{xy} = \sigma_{xy}^T + \sigma_{xy}^B, \quad (13)$$

must vanish. However, the layer Hall conductivity

$$\sigma_{xy}^L = \sigma_{xy}^T - \sigma_{xy}^B \quad (14)$$

can be nonzero.

In Fig. 7(a), we show the calculated layer Hall conductivity for bilayer CrPS₄. One can see its peak value can reach ~ 220 S/cm on the hole doping side. This indicates that although the net charge current flow vanishes, the AHE response within each layer is still quite large. Therefore, if one can break the symmetry that connects the two layers (here it is \mathcal{PT}), it will be possible to generate an imbalance between σ_{xy}^T and σ_{xy}^B and induce a finite AHE. A simplest method is by using the gate electric field.

Figure 7(c) shows the calculated layered-resolved and net AHE conductivities for bilayer CrPS₄ under a gate field of 0.02 V/nm. One observes that the gate field shifts the layered-resolved conductivities σ_{xy}^ℓ in different ways, leading to a finite AHE. In Fig. 7(d), we plot the net AHE conductivity as a function of gate field at a fix chemical potential $\mu = -0.25$ eV. One observes the linear scaling at weak field region, and the sign of AHE response can be controlled by the direction of gate field, which is a nice feature for device applications.

VII. IN-PLANE ANOMALOUS HALL EFFECT IN BILAYER

Another way to break the \mathcal{PT} symmetry of bilayer CrPS₄ is to apply an in-plane magnetic field [55]. (Out-of-plane B field also works, but it will bring in the ordinary Hall effect.) The main effect of this in-plane B field is to tilt the local magnet moments and cause a net in-plane magnetization δM along the B field direction. It was found from experiment that the magnetic anisotropy in CrPS₄ is relatively weak, so the spin canting can be readily achieved by moderate B field strength [29].

The direction of in-plane B field affects the induced AHE. For field along y direction, the resulting magnetization δM_y cannot efficiently generate AHE, because it preserves the \mathcal{M}_y symmetry for each layer. In comparison, the component δM_x along x direction is more

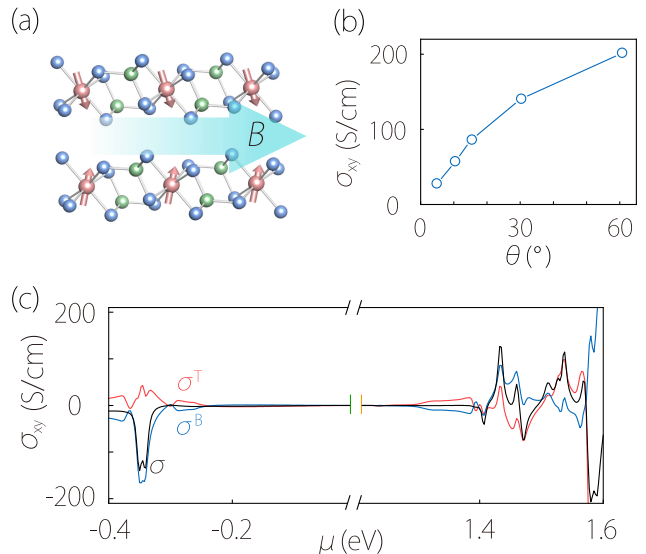


FIG. 8. (a) Schematic figure showing the application of an in-plane magnetic field to bilayer CrPS₄. The field breaks \mathcal{PT} symmetry, tilts the local moments, and induces a finite linear anomalous Hall response. (b) Calculated anomalous Hall conductivity versus spin-canting angle θ at a fixed chemical potential of -0.31 eV. (c) Calculated layer-resolved and total anomalous Hall conductivities for the bilayer when the spin-canting angle $\theta = 30^\circ$.

effective in producing the AHE response. In the following, we shall focus on the this case, with B field causing spin canting in the x direction.

In DFT calculation, we model the spin-canted state by rotating the local moments towards the x direction by a canting angle θ . At a small angle $\theta = 30^\circ$, the calculated layered-resolved and net AHE conductivities are plotted in Fig. 8(c). One observes that the contributions from the two layers no longer cancel out. A sizable AHE conductivity with peak value ~ 132 S/cm can be obtained. In Fig. 8(b), we plot the induced AHE conductivity as a function of angle canting θ for a fixed $\mu = -0.31$ eV. The curve shows a linear increase at small angles and tends to saturate at large angle. It reaches ~ 201 S/cm at angle $\theta = 60^\circ$.

The magnitude of B field needed to achieve the canting angle θ can be estimated as $B \approx 2J_c S \sin(\theta)/(g\mu_B)$. Here, we take the interlayer exchange coupling $J_c = 0.15$ meV as obtained from experiment [25], and $S = 3/2$. In this estimation, the magnetic anisotropy energy is neglected, since it is two order of magnitude smaller than the exchange energy [25]. We find that a canting angle of 5° can be achieved by a moderate B field of 340 mT, showing that using in-plane B field is an effective way to control the AHE response in bilayer CrPS₄.

VIII. DISCUSSION AND CONCLUSION

In this study, we have investigated the rich anomalous Hall transport phenomena in 2D CrPS₄ systems. Monolayer and bilayer CrPS₄ are used as representatives for demonstration. The general features apply also to other few-layer CrPS₄ systems. The odd layers share the same symmetry as monolayer, while the even layers share the same symmetry as bilayer. Hence, linear AHE is expected in odd layers, whereas nonlinear Hall effect is expected in even layers. The linear AHE induced by gate field or in-plane magnetic field should occur in even-layer CrPS₄ as well.

Experimentally, 2D CrPS₄ has been successfully fabricated via various techniques down to monolayer limit [25, 28]. Field effect transistor devices based on 2D CrPS₄ have also been demonstrated [31, 35–37]. The phenomena predicted here should be detectable via standard transport measurement with a dual gate device setup. For the nonlinear Hall effect, the typical method is to modulate the driving current with a low frequency (less than 100 Hz) and measure the response signal at second harmonic frequency by using the lock-in technique [11, 12]. The angular dependence of the signal (as manifested in Eq. (9)) can be probed by fabricating a disk shaped device with multiple leads to allow driving current (and response signal) exerted (detected) along different in-plane directions.

For odd-layer CrPS₄, the nonlinear transport signal should vanish both above and below magnetic transition temperature T_c . For even layers, the nonlinear signal is forbidden above T_c (since the crystal structure preserves \mathcal{P}) and appears only when temperature is lowered below T_c . This could be used as a signature for detecting T_c or the parity of number of layers. In addition, we note that for temperature above T_c , both linear and second-order Hall effects are forbidden by the \mathcal{T} and \mathcal{P} symmetries. The leading order anomalous Hall response should be from the third order [51, 56], which was recently probed

in several nonmagnetic materials.

In this work, we focus on the intrinsic responses, which represent inherent material properties. There also exist extrinsic contributions arising from disorder scattering, which vary from sample to sample [57]. Experimentally, a typical method to distinguish the different contributions is to perform a scaling analysis by varying the various disorder strengths. The intrinsic response correspond to a component that is independent of scattering. And first-principles result serves as an important benchmark for such analysis.

In conclusion, we have investigated various anomalous Hall transport phenomena in 2D CrPS₄. Due to their low crystal symmetry and layer-dependent magnetism, we find interesting linear and nonlinear AHEs, with sizable conductivities predicted by our first-principles calculations. These effects allow us to probe the intrinsic band geometric quantities, such as Berry curvature, BCP, and quantum metric, of the material system. The demonstrated controllability of Hall transport in 2D CrPS₄ also offers possible mechanisms for device operations. Our predications here can be readily tested in experiment, and they may find promising applications in next-generation electronics and spintronics based on 2D magnetic materials.

ACKNOWLEDGMENTS

The authors thank D. L. Deng for valuable discussions. This work is supported by UM Start-up Grant (SRG2023-00033-IAPME, SRG2022-00030-IAPME, and SRG2023-00057-IAPME), UM Multi-Year Research Grant (MYRG-GRG2023-00206-IAPME-UMDF), Science and Technology Development Fund of Macau SAR (0048/2023/RIB2 and 0066/2024/RIA1), National Key R&D Program of China (Grant No. 2022YFA1402600), and NSFC (Grants No. 12174018).

-
- [1] N. Nagaosa, J. Sinova, S. Onoda, A. H. MacDonald, and N. P. Ong, *Rev. Mod. Phys.* **82**, 1539 (2010).
 - [2] T. Jungwirth, Q. Niu, and A. H. MacDonald, *Phys. Rev. Lett.* **88**, 207208 (2002).
 - [3] M. Onoda and N. Nagaosa, *Journal of the Physical Society of Japan* **71**, 19 (2002).
 - [4] Y. Gao, S. A. Yang, and Q. Niu, *Phys. Rev. Lett.* **112**, 166601 (2014).
 - [5] C. Wang, Y. Gao, and D. Xiao, *Phys. Rev. Lett.* **127**, 277201 (2021).
 - [6] H. Liu, J. Zhao, Y.-X. Huang, W. Wu, X.-L. Sheng, C. Xiao, and S. A. Yang, *Phys. Rev. Lett.* **127**, 277202 (2021).
 - [7] H. Liu, J. Zhao, Y.-X. Huang, X. Feng, C. Xiao, W. Wu, S. Lai, W.-b. Gao, and S. A. Yang, *Phys. Rev. B* **105**, 045118 (2022).
 - [8] A. Gao, Y.-F. Liu, J.-X. Qiu, B. Ghosh, T. V. Trevisan, Y. Onishi, C. Hu, T. Qian, H.-J. Tien, S.-W. Chen, M. Huang, D. Bérubé, H. Li, C. Tzschaschel, T. Dinh, Z. Sun, S.-C. Ho, S.-W. Lien, B. Singh, K. Watanabe, T. Taniguchi, D. C. Bell, H. Lin, T.-R. Chang, C. R. Du, A. Bansil, L. Fu, N. Ni, P. P. Orth, Q. Ma, and S.-Y. Xu, *Science* **381**, 181 (2023).
 - [9] X. Feng, W. Wu, H. Wang, W. Gao, L. K. Ang, Y. Zhao, C. Xiao, and S. A. Yang, [arXiv:2402.00532](https://arxiv.org/abs/2402.00532).
 - [10] I. Sodemann and L. Fu, *Phys. Rev. Lett.* **115**, 216806 (2015).
 - [11] Q. Ma, S.-Y. Xu, H. Shen, D. MacNeill, V. Fatemi, T.-R. Chang, A. M. Mier Valdivia, S. Wu, Z. Du, C.-H. Hsu, S. Fang, Q. D. Gibson, K. Watanabe, T. Taniguchi, R. J. Cava, E. Kaxiras, H.-Z. Lu, H. Lin, L. Fu, N. Gedik, and P. Jarillo-Herrero, *Nature* **565**, 337 (2019).
 - [12] K. Kang, T. Li, E. Sohn, J. Shan, and K. F. Mak, *Nature Materials* **18**, 324 (2019).

- [13] Z. Z. Du, H.-Z. Lu, and X. C. Xie, *Nature Reviews Physics* **3**, 744 (2021).
- [14] N. Wang, D. Kaplan, Z. Zhang, T. Holder, N. Cao, A. Wang, X. Zhou, F. Zhou, Z. Jiang, C. Zhang, S. Ru, H. Cai, K. Watanabe, T. Taniguchi, B. Yan, and W. Gao, *Nature* **621**, 487 (2023).
- [15] J. Han, T. Uchimura, Y. Araki, J.-Y. Yoon, Y. Takeuchi, Y. Yamane, S. Kanai, J. Ieda, H. Ohno, and S. Fukami, *Nature Physics* **20**, 1110 (2024).
- [16] K. S. Burch, D. Mandrus, and J.-G. Park, *Nature* **563**, 47 (2018).
- [17] K. F. Mak, J. Shan, and D. C. Ralph, *Nature Reviews Physics* **1**, 646 (2019).
- [18] H. Kurebayashi, J. H. Garcia, S. Khan, J. Sinova, and S. Roche, *Nature Reviews Physics* **4**, 150 (2022).
- [19] B. Huang, G. Clark, E. Navarro-Moratalla, D. R. Klein, R. Cheng, K. L. Seyler, D. Zhong, E. Schmidgall, M. A. McGuire, D. H. Cobden, W. Yao, D. Xiao, P. Jarillo-Herrero, and X. Xu, *Nature* **546**, 270 (2017).
- [20] Y. Deng, Y. Yu, Y. Song, J. Zhang, N. Z. Wang, Z. Sun, Y. Yi, Y. Z. Wu, S. Wu, J. Zhu, J. Wang, X. H. Chen, and Y. Zhang, *Nature* **563**, 94 (2018).
- [21] Z. Fei, B. Huang, P. Malinowski, W. Wang, T. Song, J. Sanchez, W. Yao, D. Xiao, X. Zhu, A. F. May, W. Wu, D. H. Cobden, J.-H. Chu, and X. Xu, *Nature Materials* **17**, 778 (2018).
- [22] C. Gong, L. Li, Z. Li, H. Ji, A. Stern, Y. Xia, T. Cao, W. Bao, C. Wang, Y. Wang, Z. Q. Qiu, R. J. Cava, S. G. Louie, J. Xia, and X. Zhang, *Nature* **546**, 265 (2017).
- [23] S. Yang, X. Xu, Y. Zhu, R. Niu, C. Xu, Y. Peng, X. Cheng, X. Jia, Y. Huang, X. Xu, J. Lu, and Y. Ye, *Phys. Rev. X* **11**, 011003 (2021).
- [24] D. Ovchinnikov, X. Huang, Z. Lin, Z. Fei, J. Cai, T. Song, M. He, Q. Jiang, C. Wang, H. Li, Y. Wang, Y. Wu, D. Xiao, J.-H. Chu, J. Yan, C.-Z. Chang, Y.-T. Cui, and X. Xu, *Nano Letters* **21**, 2544 (2021).
- [25] J. Son, S. Son, P. Park, M. Kim, Z. Tao, J. Oh, T. Lee, S. Lee, J. Kim, K. Zhang, K. Cho, T. Kamiyama, J. H. Lee, K. F. Mak, J. Shan, M. Kim, J.-G. Park, and J. Lee, *ACS Nano* **15**, 16904 (2021).
- [26] Q. L. Pei, X. Luo, G. T. Lin, J. Y. Song, L. Hu, Y. M. Zou, L. Yu, W. Tong, W. H. Song, W. J. Lu, and Y. P. Sun, *Journal of Applied Physics* **119**, 043902 (2016).
- [27] H. L. Zhuang and J. Zhou, *Phys. Rev. B* **94**, 195307 (2016).
- [28] J. Lee, T. Y. Ko, J. H. Kim, H. Bark, B. Kang, S.-G. Jung, T. Park, Z. Lee, S. Ryu, and C. Lee, *ACS Nano* **11**, 10935 (2017).
- [29] Y. Peng, S. Ding, M. Cheng, Q. Hu, J. Yang, F. Wang, M. Xue, Z. Liu, Z. Lin, M. Avdeev, Y. Hou, W. Yang, Y. Zheng, and J. Yang, *Advanced Materials* **32**, 2001200 (2020).
- [30] S. Calder, A. V. Haglund, Y. Liu, D. M. Pajerowski, H. B. Cao, T. J. Williams, V. O. Garlea, and D. Mandrus, *Phys. Rev. B* **102**, 024408 (2020).
- [31] R. Wu, A. Ross, S. Ding, Y. Peng, F. He, Y. Ren, R. Lebrun, Y. Wu, Z. Wang, J. Yang, A. Brataas, and M. Kläui, *Phys. Rev. Appl.* **17**, 064038 (2022).
- [32] M. Riesner, R. Fainblat, A. K. Budniak, Y. Amouyal, E. Lifshitz, and G. Bacher, *The Journal of Chemical Physics* **156**, 054707 (2022).
- [33] S. Kim, S. Yoon, H. Ahn, G. Jin, H. Kim, M.-H. Jo, C. Lee, J. Kim, and S. Ryu, *ACS Nano* **16**, 16385 (2022).
- [34] N. C. Harms, K. A. Smith, A. V. Haglund, D. G. Mandrus, Z. Liu, H.-S. Kim, and J. L. Musfeldt, *ACS Applied Electronic Materials* **4**, 3246 (2022).
- [35] F. Wu, M. Gibertini, K. Watanabe, T. Taniguchi, I. Gutiérrez-Lezama, N. Ubrig, and A. F. Morpurgo, *Advanced Materials* **35**, 2211653 (2023).
- [36] F. Wu, M. Gibertini, K. Watanabe, T. Taniguchi, I. Gutiérrez-Lezama, N. Ubrig, and A. F. Morpurgo, *Nano Letters* **23**, 8140 (2023).
- [37] M. Cheng, Q. Hu, Y. Huang, C. Ding, X.-B. Qiang, C. Hua, H. Fang, J. Lu, Y. Peng, J. Yang, C. Xi, L. Pi, K. Watanabe, T. Taniguchi, H.-Z. Lu, K. S. Novoselov, Y. Lu, and Y. Zheng, *Nature Physics* , 1 (2024).
- [38] M. Huang, J. C. Green, J. Zhou, V. Williams, S. Li, H. Lu, D. Djugba, H. Wang, B. Flebus, N. Ni, and C. R. Du, *Nano Letters* **23**, 8099 (2023).
- [39] G. Kresse and J. Hafner, *Phys. Rev. B* **47**, 558 (1993).
- [40] G. Kresse and J. Furthmüller, *Comput. Mater. Sci.* **6**, 15 (1996).
- [41] G. Kresse and J. Furthmüller, *Phys. Rev. B* **54**, 11169 (1996).
- [42] P. E. Blöchl, *Phys. Rev. B* **50**, 17953 (1994).
- [43] J. P. Perdew, J. A. Chevary, S. H. Vosko, K. A. Jackson, M. R. Pederson, D. J. Singh, and C. Fiolhais, *Phys. Rev. B* **46**, 6671 (1992).
- [44] J. P. Perdew, K. Burke, and M. Ernzerhof, *Phys. Rev. Lett.* **77**, 3865 (1996).
- [45] S. Grimme, J. Antony, S. Ehrlich, and H. Krieg, *J. Chem. Phys.* **132**, 154104 (2010).
- [46] S. L. Dudarev, G. A. Botton, S. Y. Savrasov, C. J. Humphreys, and A. P. Sutton, *Phys. Rev. B* **57**, 1505 (1998).
- [47] A. A. Mostofi, J. R. Yates, G. Pizzi, Y.-S. Lee, I. Souza, D. Vanderbilt, and N. Marzari, *Comput. Phys. Commun.* **185**, 2309 (2014).
- [48] A. Louisy, G. Ouvrard, D. Schleich, and R. Brec, *Solid State Communications* **28**, 61 (1978).
- [49] T. Jungwirth, Q. Niu, and A. H. MacDonald, *Phys. Rev. Lett.* **88**, 207208 (2002).
- [50] Y. Yao, L. Kleinman, A. H. MacDonald, J. Sinova, T. Jungwirth, D.-s. Wang, E. Wang, and Q. Niu, *Phys. Rev. Lett.* **92**, 037204 (2004).
- [51] S. Lai, H. Liu, Z. Zhang, J. Zhao, X. Feng, N. Wang, C. Tang, Y. Liu, K. Novoselov, S. A. Yang, and W.-b. Gao, *Nature Nanotechnology* **16**, 869 (2021).
- [52] A. Gao, S.-W. Chen, B. Ghosh, J.-X. Qiu, Y.-F. Liu, Y. Onishi, C. Hu, T. Qian, D. Bérubé, T. Dinh, H. Li, C. Tzschaschel, S. Park, T. Huang, S.-W. Lien, Z. Sun, S.-C. Ho, B. Singh, K. Watanabe, T. Taniguchi, D. C. Bell, A. Bansil, H. Lin, T.-R. Chang, A. Yacoby, N. Ni, L. Fu, Q. Ma, and S.-Y. Xu, *Nature Electronics* **7**, 751 (2024).
- [53] A. Gao, Y.-F. Liu, C. Hu, J.-X. Qiu, C. Tzschaschel, B. Ghosh, S.-C. Ho, D. Bérubé, R. Chen, H. Sun, Z. Zhang, X.-Y. Zhang, Y.-X. Wang, N. Wang, Z. Huang, C. Felser, A. Agarwal, T. Ding, H.-J. Tien, A. Akey, J. Gardener, B. Singh, K. Watanabe, T. Taniguchi, K. S. Burch, D. C. Bell, B. B. Zhou, W. Gao, H.-Z. Lu, A. Bansil, H. Lin, T.-R. Chang, L. Fu, Q. Ma, N. Ni, and S.-Y. Xu, *Nature* **595**, 521 (2021).
- [54] F.-R. Fan, C. Xiao, and W. Yao, *Nature Communications* **15**, 7997 (2024).
- [55] J. Cao, W. Jiang, X.-P. Li, D. Tu, J. Zhou, J. Zhou, and Y. Yao, *Phys. Rev. Lett.* **130**, 166702 (2023).
- [56] C. Wang, R.-C. Xiao, H. Liu, Z. Zhang, S. Lai, C. Zhu,

H. Cai, N. Wang, S. Chen, Y. Deng, Z. Liu, S. A. Yang, and W.-B. Gao, [National Science Review](#) **9**, nwac020 (2022).

[57] Y.-X. Huang, C. Xiao, S. A. Yang, and X. Li, [arXiv:2311.01219](#).